Improvement of Corona Breakdown Threshold (Peak Power Handling) in Smooth-Profiled Microstrip Filters

Jamil Ahmad[1], Jabir Hussain[1], Ivan Arregui[1], Petronilo Martin-Iglesias[2], Israel Arnedo[1], Miguel A. G. Laso[1] and Txema Lopetegi[1]

[1] Institute of Smart Cities (ISC), Department of Electrical, Electronic and Communications Engineering, Public University of Navarre (UPNA), Campus Arrosadia, 31006 Pamplona, Spain.

jamil.ahmad@unavarra.es, jabir.hussain@unavarra.es, ivan.arregui@unavarra.es israel.arnedo@unavarra.es, mangel.gomez@unavarra.es, txema.lopetegi@unavarra.es

[2] European Space Research and Technology Centre, European Space Agency (ESTEC-ESA), 2201 AZ Noordwijk, The Netherlands.

petronilo.martin.iglesias@esa.int

INTRODUCTION

Microstrip circuits have been widely used in huge number of applications. Their low volume, weight and cost make them an attractive solution to design multiple passive components such as dividers, couplers and filters. In contrast to strip line, there is easy-to-use microstrip technology for building multifunctional devices. Recent advances in material science have given rise to high-k substrates, which are helping researchers to design low loss microstrip circuits. Moreover, solid-state power amplifier (SSPA) has made it possible to use microstrip technology at the outer stages of high power transmitters. Therefore, special attention needs to be paid to the power handling capability of the microstrip circuits. Multipactor and corona effect are two major phenomena that arise with the strength of electric field [1-3]. Corona effect or gas breakdown results from the high electric field strength in the air giving rise to different physical phenomena [4-5]. The specific region of the microstrip circuit featuring the stronger electric field ionizes the gas molecules (e.g., air), heats up the component and eventually destroys the device.

Microwave filters are key components of any communication system at both transmitter and receiver ends. Filter is a two-port network, which only passes the band of interest and rejects the undesired frequencies. Among the classical filter design techniques [6-9], insertion loss method has been widely used as a classical synthesis approach based on discrete components. Since the discrete components are suitable only for low frequencies, distributed filter networks were developed to operate at high frequencies. The equivalence between discrete elements and distributed networks is exact only at a single operating frequency. In microstrip low-pass distributed networks, N (filter order) steps of metal strips of different width (characteristic impedance) are connected to achieve the desired response. However, there are various demerits for the classical stepped-impedance technique, i.e., spurious bands, excitation of higher order modes, lack of control on out of band response and poor selectivity. The concept of smooth-profiled structure designed by employing inverse scattering synthesis techniques was reported by Arnedo et al. [10]. Although the sharp edges of the stepped-impedance filter were replaced by smooth transitions of the strip, the reported techniques were limited to only rational functions in terms of the reflection response with a long length of the device, or to moderate maximum reflectivities (moderate maximum attenuations in the rejected band). In order to overcome these limitations having full control over the length of the device, the continuous layer peeling inverse scattering technique was proposed and employed in [11] to extract the coupling coefficient profile of the device by peeling off the successive layers of differential thickness, and the associated smooth impedance profile for the filter was obtained.

STEPPED-IMPEDANCE FILTER

Stepped-impedance filter is a conventional filter design technique implemented by cascading N unit elements of equal electrical lengths that is termed as commensurate line filter. The distributed network is derived by invoking Richards' transformation [12-14] as illustrated in fig.1. The impedances of these unit elements are calculated by using the [ABCD] transfer matrix [1].

$$\begin{bmatrix} A & B \\ C & D \end{bmatrix}_{UE} = \frac{1}{\sqrt{1-t^2}} \begin{bmatrix} 1 & Z_0 t \\ t/Z_0 & 1 \end{bmatrix} \quad (1)$$

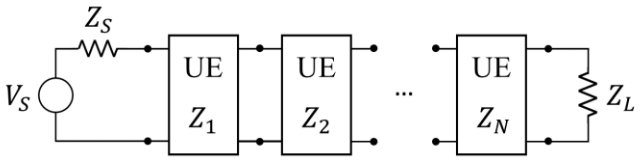

Fig. 1. Commensurate-line distributed prototype represented in the Richards' transformation domain as a cascade of N UEs

Once the impedance profile is obtained, commercially available software, ADS Linecalc is employed to extract the microstrip width for the corresponding impedance profile. Hence, a classical stepped-impedance filter is achieved featuring equal electrical length of all the unit sections.

These cascaded unit elements feature sharp edges at the 90-degree transition, which concentrate the electric field at the edges and eventually increase the strength of the electric field. A high electric field ionizes the gas molecules (i.e., air) and corona discharge appears at low power levels, in other words, the peak power handling capability (PPHC) of the device reduces.

For the given specifications of the filter, in terms of insertion loss (IL), return loss (RL), cut off frequency f_c, and frequency of maximum rejection f_0, the order of the filter (N) for Chebyshev response can be calculated as follows:

$$N = \frac{\operatorname{acosh}\sqrt{\left(\frac{1}{|S21|^2_{min}}-1\right).\left(10^{\frac{RL}{10}}-1\right)}}{\operatorname{asech}\left(\frac{1}{\alpha}\right)} \qquad (2)$$

where $|S21|_{min}$ is the minimum value of the S_{21} transmission parameter at frequency f_0 and $\alpha = \frac{1}{\sin\theta_c}$, where θ_c is the electrical length of the commensurate lines at the cut off frequency f_c.

SMOOTH-PROFILED FILTER

If the sharp corners of the device are replaced by rounded corners, the electric field strength of the device reduces, which in turn increases the PPHC [15]. The classical stepped-impedance filter provides the base to design the novel smooth-profiled microstrip filter featuring the same physical length of the classical device. The inverse scattering technique "continuous layer peeling (CLP)" is employed to get the smooth profile. A brief summary of the design methodology is following:

Step 1: For the given filter specifications, the order of the filter, N is calculated with (2).

Step 2: The impedance values of the N unit element sections are calculated using [ABCD] transfer matrix (1).

Step 3: The frequency response of the whole device is computed by multiplying the transfer matrices of the N cascaded unit elements.

Step 4: The frequency response obtained in Step 3 features periodic rejection bands. The S_{11} response of the UE is truncated by nullifying the S_{11} parameters beyond $2f_0$. It results in an ideal frequency response with no spurious rejection bands and it will serve as target response for the CLP synthesis algorithm.

Step 5: In the modified target frequency response, the CLP algorithm is applied to synthesize the coupling coefficient. Initially CLP is applied at the origin of the device ($z = 0$), first infinitesimal layer to get the coupling coefficient $K(0)$ by using (3).

$$K(z=0) = -\frac{4}{\pi}\int_0^\infty \mathrm{Re}\{S_{11}(\beta)\} \cdot d\beta. \qquad (3)$$

Step 6: Once the initial coupling coefficient $K(0)$ is evaluated, Riccati equation (4) is used to propagate the reflection coefficient along the first layer of the device. Now the first layer is peeled off and the origin of the device is shifted to next layer. Then, the next point of the coupling coefficient can be calculated using (3). Following in an iterative manner, i.e., propagating the target spectrum with (4) and calculating the next value of

the coupling coefficient by means of (3), the entire coupling coefficient $K(z)$ for the smooth profile device is synthesized.

$$\frac{d\rho}{dz} = 2 \cdot j \cdot \beta \cdot \rho + K \cdot (1 - \rho 2) \qquad (4)$$

Step 7: Finally, the characteristic impedance profile corresponding to the coupling coefficient calculated in Step 6 is computed by using the analytical expression (5).

$$Z_0(z) = Z_0(0).e^{-2\int_0^z K(g).dg} \qquad (5)$$

$Z_0(0)$ is the value of the characteristic impedance at the input port, and g is a dummy variable to calculate the integral. ADS Linecalc is used to extract the width profile of the strip. Fig. 2 illustrates the impedance profiles of both stepped-impedance and smooth-profile for seven-order chebyshev filter.

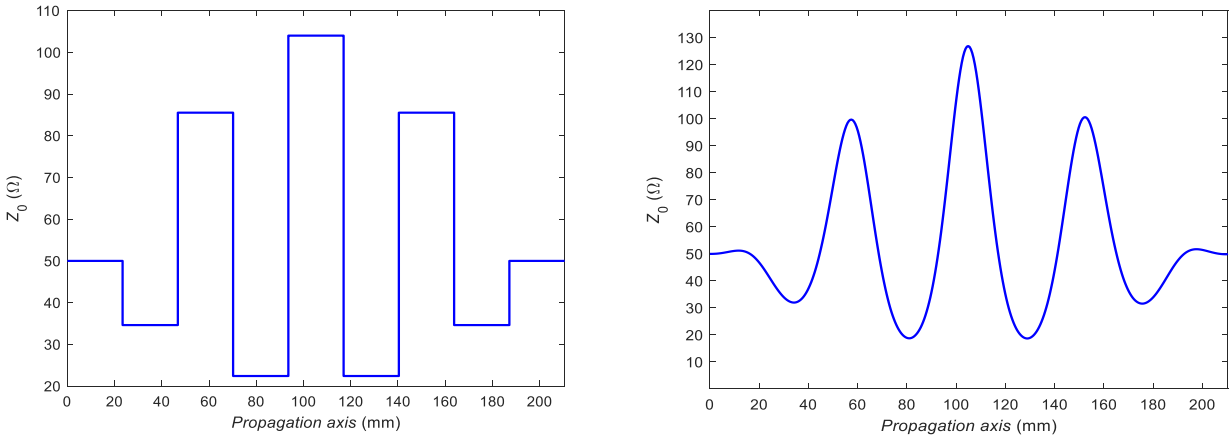

(a) (b)

Fig. 2. Characteristic impedance of the seven-order Chebyshev filter along the propagation direction: (a) Stepped-impedance filter, (b) Smooth-profiled filter

DESIGN EXAMPLES

In order to compare the performance of the stepped-impedance (SI) and smooth-profile (SP) techniques, four filter prototypes are designed, with the design specifications listed in the Table 1. For each of the prototypes, Rogers 3035 substrate with relative electric permittivity $\varepsilon_r = 3.5$ was employed with a thickness of $h = 1.524$ mm.

Table 1. Specifications of Designed Prototypes

	$Insertion\ loss = 30$ dB $Return\ Loss = 20$ dB $filter\ order = 7$ $substrate\ h = 1.524$ mm	
Prototype No.	f_c(GHz)	f_0(GHz)
1	0.447	1
2	0.9	2
3	1.3	3
4	1.78	4

The four prototypes are simulated with CST Studio Suite 2020, the layouts of the SP and SI prototypes are presented in Fig. 3. In order to make a fair comparison, the S-parameters of both techniques are compared in Fig. 4, to make sure that the corresponding designs feature the same cut-off frequency as intended.

(a) (b)

Fig. 3. Microstrip profile: (a) Stepped-impedance filter, (b) Smooth-profiled filter

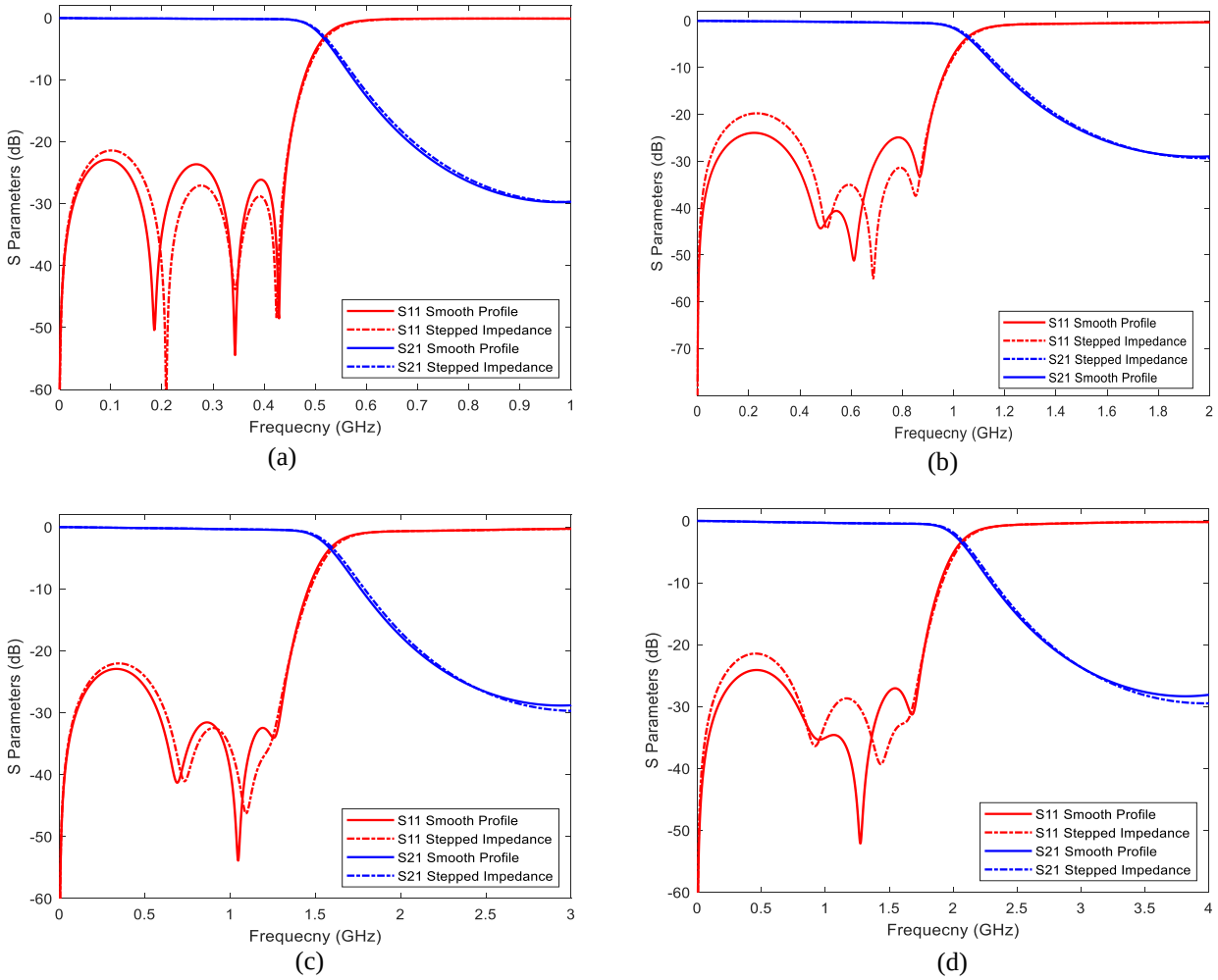

Fig. 4. CST simulated S-parameter results: (a) Prototype 1, (b) Prototype 2, (c) Prototype 3, (d) Prototype 4

Since the voltage magnification is maximum at the cut-off frequency [16], the electric fields of the four prototypes are computed at the cut-off frequencies. In the stepped-impedance filters, it is observed that most of the electric field is accumulated at the sharp corners of the strip, whereas in the smooth-profiled filters, the presence of smooth transitions avoids the concentration of the electric fields. The electric field patterns for both SI and SP filters are presented in Fig. 5 to visualize this effect. Moreover, to further investigate the electric field phenomena, 1D plots of E-field magnitude along the strip contour are displayed in Fig. 6.

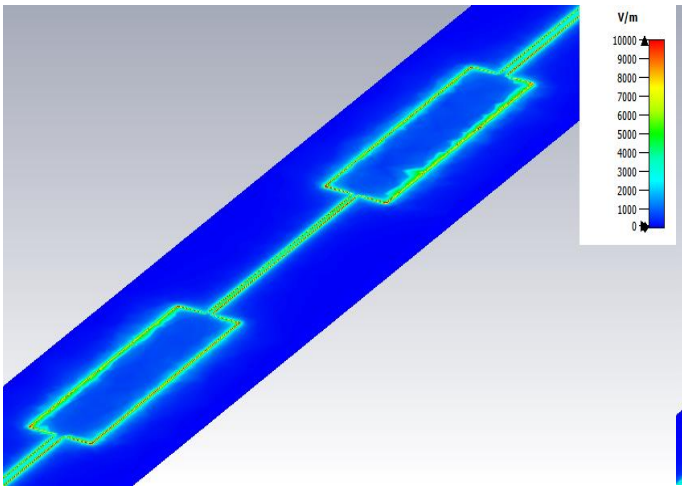
V/m
10000
9000
8000
7000
6000
5000
4000
3000
2000
1000
0

(a)

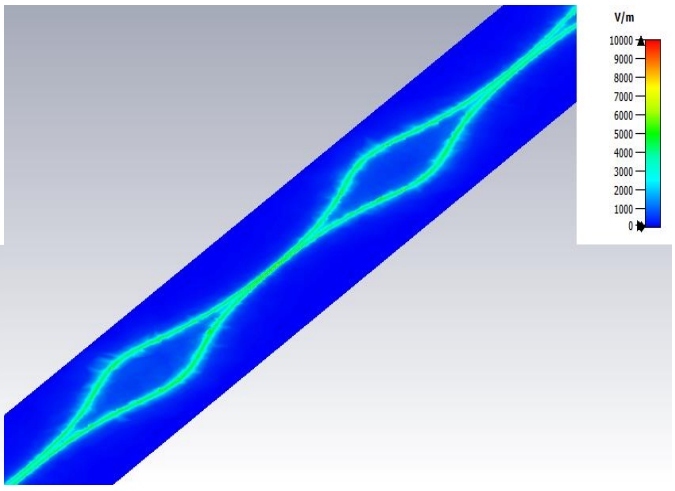
V/m
10000
9000
8000
7000
6000
5000
4000
3000
2000
1000
0

(b)

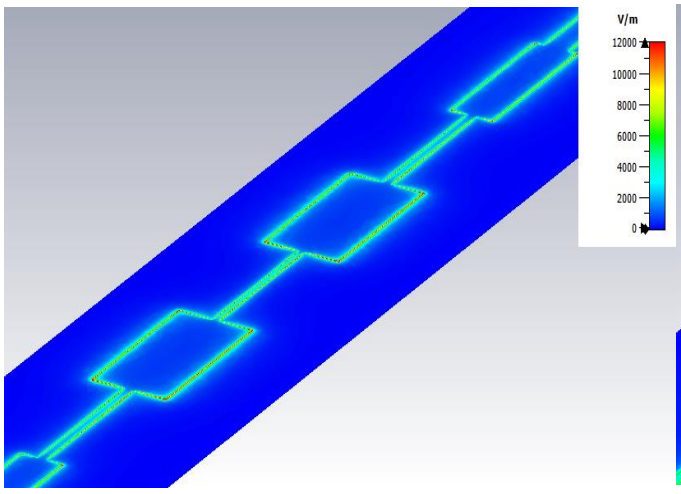
V/m
12000
10000
8000
6000
4000
2000
0

(c)

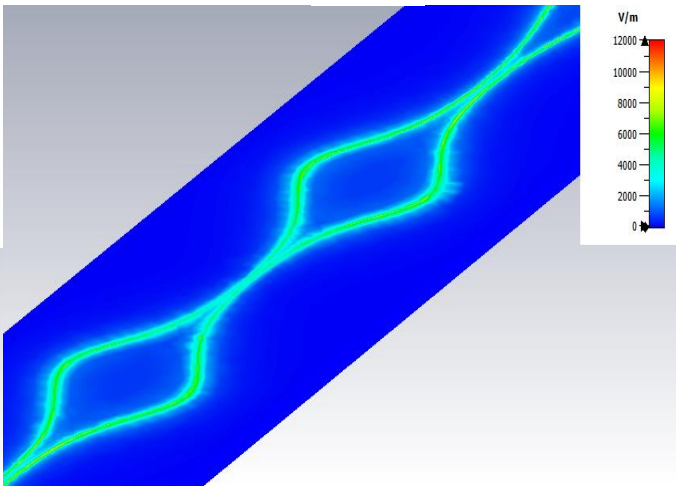
V/m
12000
10000
8000
6000
4000
2000
0

(d)

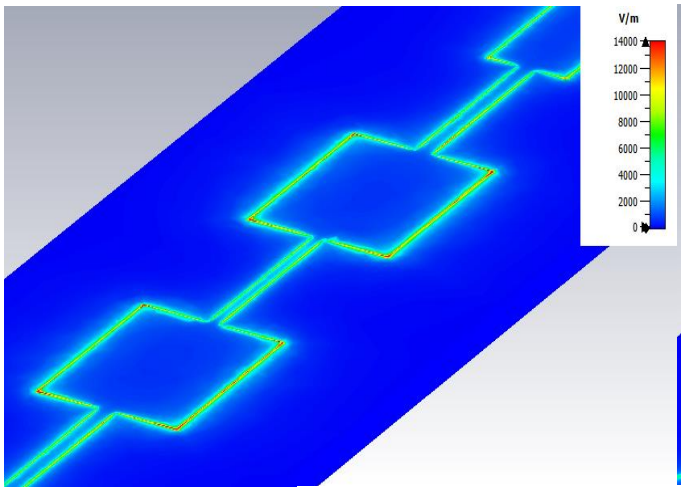
V/m
14000
12000
10000
8000
6000
4000
2000
0

(e)

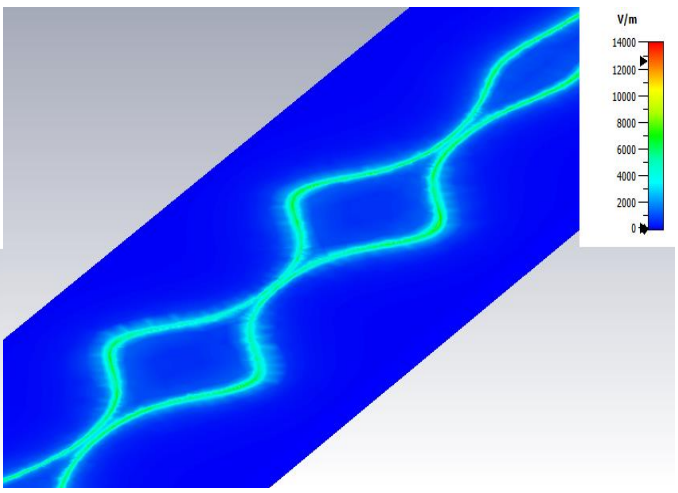
V/m
14000
12000
10000
8000
6000
4000
2000
0

(f)

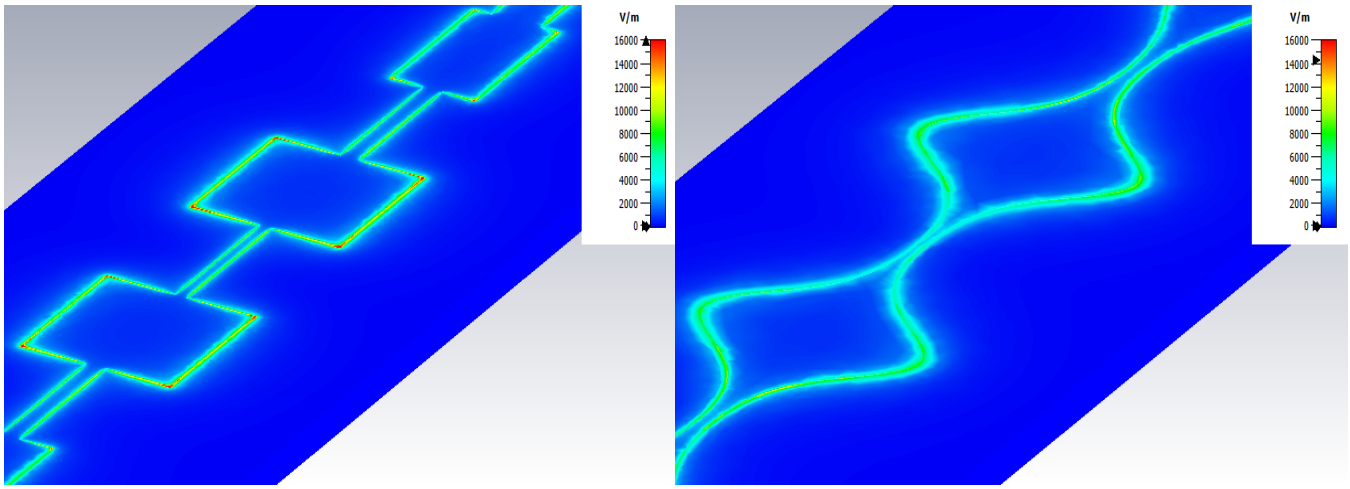

(g) (h)

Fig. 5. Electric field pattern: (a) Prototype 1, SI. (b) Prototype 1, SP. (c) Prototype 2, SI. (d) Prototype 2, SP. (e) Prototype 3, SI. (f) Prototype 3, SP. (g) Prototype 4, SI. (h) Prototype 4, SP

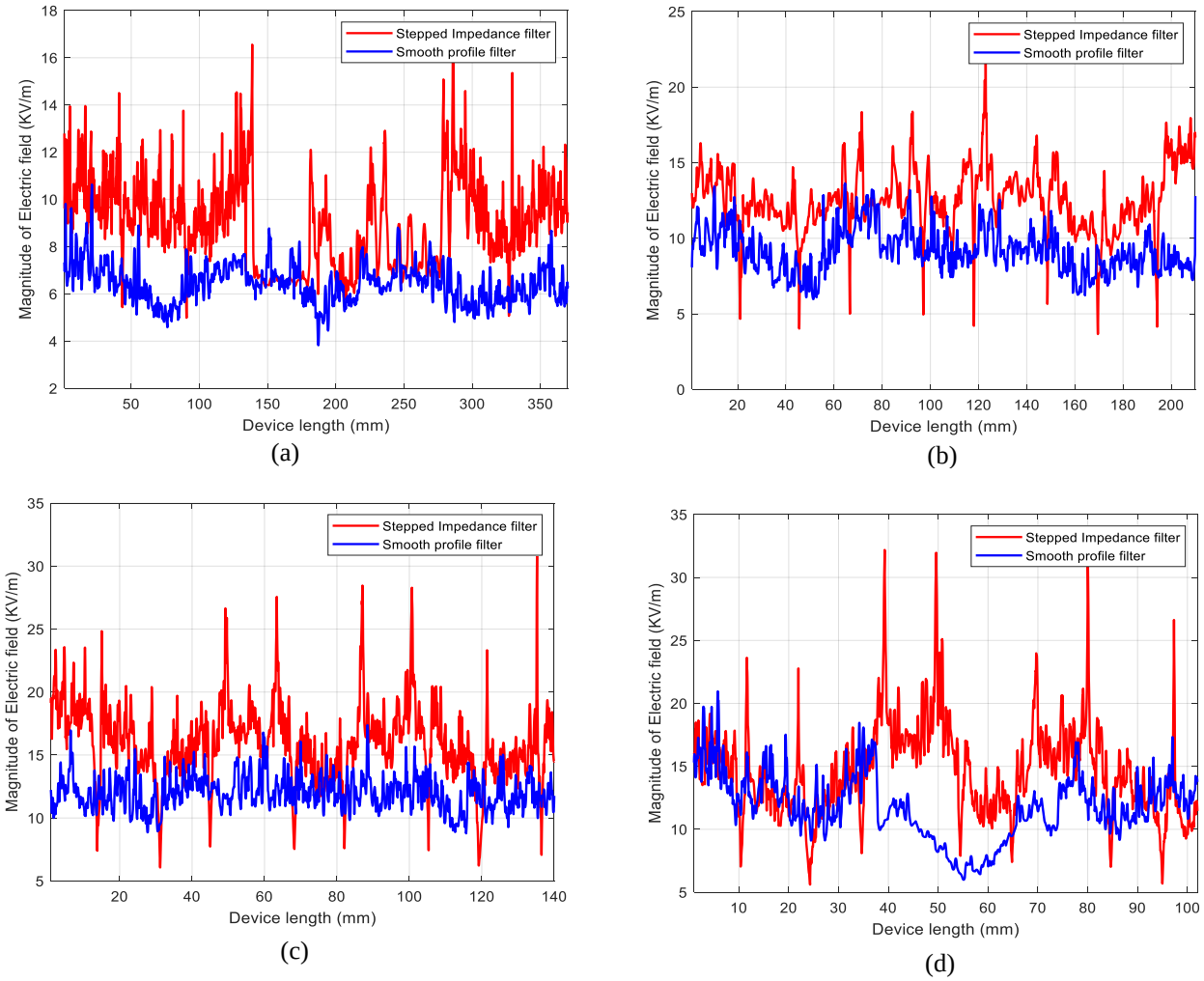

Fig. 6. Electric field 1D plot along the strip contour: (a) Prototype 1, (b) Prototype 2, (c) Prototype 3, (d) Prototype 4

CORONA ANALYSIS

The electric fields calculated at the cut-off frequencies of the filters with CST, are exported to the commercial software tool SPARK3D, where corona breakdown is analyzed for the pressure range 0.1mbar – 1000mbar. Inspecting the corona breakdown results presented in Fig. 7, it is clear that the PPHC is much better for the smooth-profiled filters than for their stepped-impedance counterparts, except for very or extremely low pressure values (always below the critical pressure) where the PPHCs tend to become roughly equal. In all the prototypes, the corona breakdown threshold at critical pressure is higher for smooth-profiled filters than for stepped-impedance filters. In the same way, in all the prototypes, the corona breakdown threshold at high pressures is higher for the smooth-profiled filters. A comparison of the PPHC values for the smooth-profiled and stepped-impedance filters, both at critical and ambient pressures, is given in Table 2.

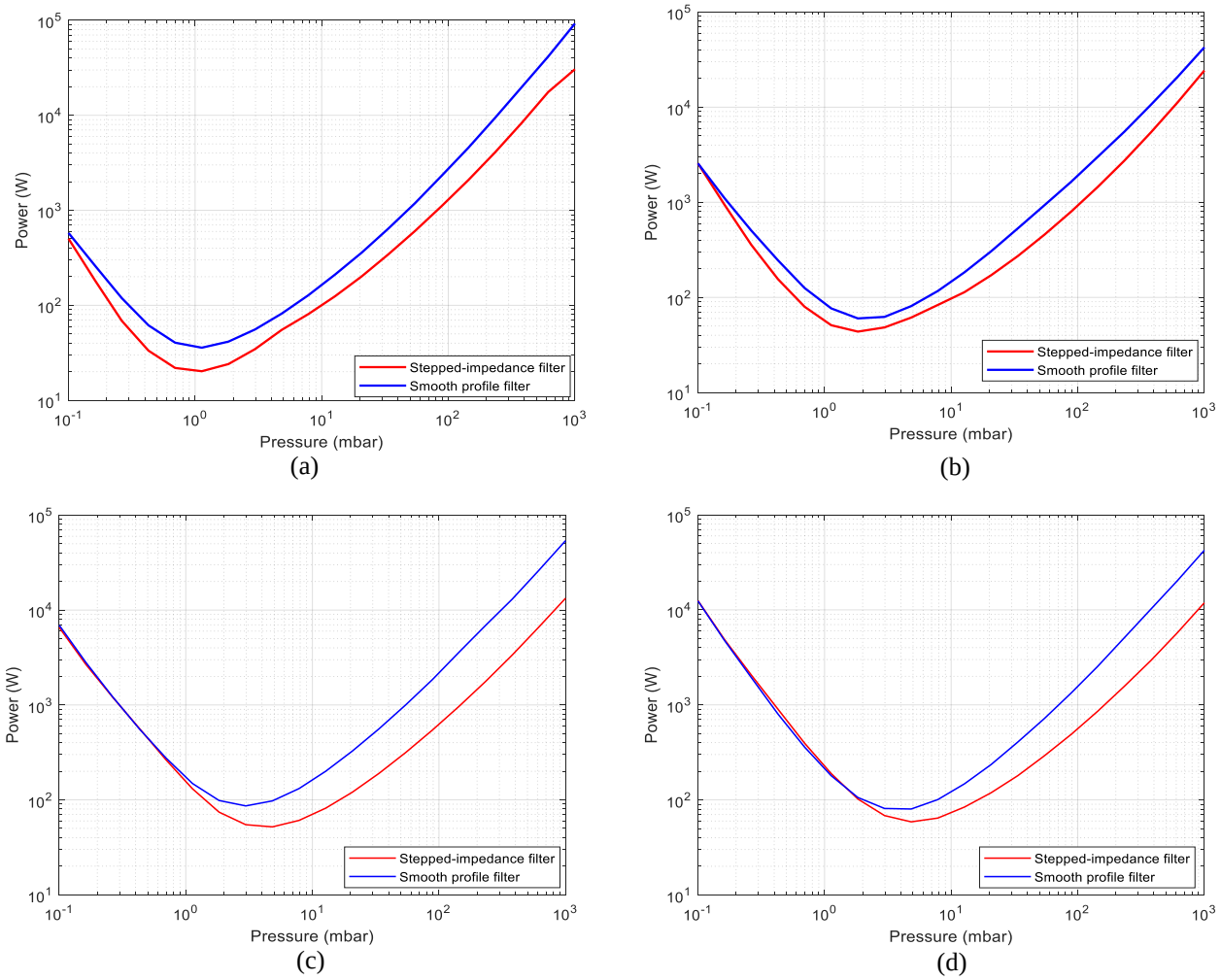

Fig. 7. Paschen curves (Corona discharge breakdown): (a) Prototype 1, (b) Prototype 2, (c) Prototype 3, (d) Prototype 4

Table 2. Corona breakdown values at critical and ambient pressures

Prototype No.	PPHC at critical pressure		PPHC enhancement at critical pressure	PPHC at ambient pressure (1000mbar)		PPHC enhancement at ambient pressure
	SI	SP		SI	SP	
1	20.25 W (1.13mbar)	35.81 W (1.13mbar)	2.47 dB	30510 W	92210 W	4.80 dB
2	43.67 W (1.83mbar)	60.12 W (1.83mbar)	1.39 dB	24280 W	42580 W	2.44 dB
3	51.90 W (4.83mbar)	86.33 W (2.97mbar)	2.21 dB	13330 W	53910 W	6.07 dB
4	58.74 W (4.83mbar)	80.17 W (4.83mbar)	1.35 dB	11870 W	42370 W	5.53 dB

CONCLUSION

In this paper, the PPHCs of two filter design techniques, stepped-impedance (SI) and smooth-profile (SP), are presented for four design prototypes. Smooth-profiled filters feature smooth variations in the characteristic impedance profile, avoiding sharp edges, which accumulate electric fields. The absence of sharp edges in SP reduces the voltage magnification factor, which in turn improves the PPHC of the filter. The phenomenon of electric fields accumulation at the sharp corners of the SI filters is presented and compared with smooth transitions in SP filters. Furthermore, 1D graphs of electric field intensity are presented along the strip contour of the microstrip lines. Finally, SPARK3D results clearly demonstrate that SP filters can handle higher peak powers than their SI counterparts between critical pressure and ambient pressure, for all the studied designs.

ACKNOWLEDGMENT

This work was supported by the Spanish Ministerio de Ciencia e Innovación –Agencia Estatal de Investigación (MCIN/AEI/10.13039/501100011033) under Project PID2020-112545RB-C53 and by the European Union's Horizon 2020 Research and Innovation Program under Grant 811232-TESLA-H2020-MSCA-ITN-2018. Jamil Ahmad also acknowledges the funding received through the PRE2018-085491 grant.

REFERENCES:

[1] R. J. Cameron, C. M. Kudsia, and R. R. Mansour, *Microwave Filters for Communication Systems*, 2nd ed., Somerset, U.K.: Wiley, 2018.
[2] M. Yu, "Power-handling capability for RF filters," *IEEE Microw. Mag.*, vol. 8, no. 5, pp. 88–97, Oct. 2007.
[3] D. Anderson, U. Jordon, M. Lisak, T. Olsson, and M. Ahlander, "Microwave breakdown in resonators and filters," *IEEE Trans. Microw. Theory Techn.*, vol. 47, no. 12, pp. 2547–2556, Dec. 1999.
[4] A. D. MacDonald, *Microwave Breakdown in Gases*. New York, NY, USA: Wiley, 1966.
[5] Y. P. Raizer, *Gas Discharge Physics*. Berlin, Germany: Springer, 1991.
[6] R. Levy and S. B. Cohn, "A history of microwave filter research, design, and development," *IEEE Trans. Microwave Theory Tech.*, vol. 32, no. 9, pp. 1055- 1067, Sept. 1984.
[7] R. Levy, R. V. Snyder, and G. Matthaei, "Design of Microwave Filters," *IEEE Trans. Microwave Theory Tech.*, vol. 50, no. 3, pp. 783-793, Mar. 2002.
[8] I. C. Hunter, L. Billonet, B. Jarry, and P. Guillon, "*Microwave Filters – Applications and Technology*," IEEE Trans. Microwave Theory Tech., vol. 50, no. 3, pp. 794-805, Mar. 2002.
[9] G. Matthaei, L. Young, E. M. T. Jones, *Microwave filters, impedance-matching networks, and coupling structures*, Artech House, Inc., 1980.
[10] I. Arnedo, I. Arregui, M. Chudzik, F. Teberio, A. Lujambio, D. Benito, T. Lopetegi, and M. A. G. Laso, "Direct and Exact Synthesis: Controlling the Microwaves by Means of Synthesized Passive Components with Smooth Profiles," *IEEE Microwave Magazine*, vol. 16, no. 4, pp. 114-128, May 2015.
[11] I. Arnedo, M. Chudzik, J. M. Percaz, I. Arregui, F. Teberio, D. Benito, T. Lopetegi, and M. A. G. Laso, "Synthesis of one dimensional electromagnetic bandgap structures with fully controlled parameters," *IEEE Trans. Microw. Theory Techn*., vol. 65, no. 9, pp. 3123-3134, Sept. 2017.
[12] P. I. Richards, "Resistor-transmission-line circuits," *Proc. IRE*, vol. 36, no. 2, pp. 217-220, Feb. 1948.
[13] H. J. Carlin, P. P. Civalleri, *Wideband Circuit Design*. Boca Raton, FL, USA: CRC Press, 1998
[14] H. Baher, *Synthesis of Electrical Networks*. New York, NY, USA: John Wiley & Sons, 1984.
[15] A. M. Morales-Hernández et al., "Increasing peak power handling in microstrip bandpass filter by using rounded-end resonantors, *IEEE Microw. Wireless Compon. Lett*., vol. 31, no. 3, pp. 237–240, March. 2021
[16] M. A. Sánchez-Soriano et al., "Peak and average power handling capability of microstrip filters," *IEEE Trans. Microw. Theory Techn*., vol. 67, no. 8, pp. 3436–3448, Aug. 2019.